Experimental study of turbulent Bluff-Body flames stability by simultaneous high speed flame imaging and Particle Image Velocimetry

Nelson Valdez, Corine Lacour, Bertrand Lecordier, Armelle Cessou, David Honoré

Experimental study of turbulent Bluff-Body flames stability by simultaneous high speed flame imaging and Particle Image Velocimetry

Nelson VALDEZ, Corine LACOUR, Bertrand LECORDIER, Armelle CESSOU, David HONORE

david.honore@coria.fr
Normandie Univ, INSA Rouen, UNIROUEN, CNRS, CORIA, 76000 Rouen, France

Abstract
Development of innovative combustion regimes improving energy efficiency and limiting pollutant emissions requires better knowledge of the limits of turbulent flame stability and of the physical phenomena controlling them. The present work is focused on the description and the quantification of intermittent phenomena occurring in non-premixed turbulent flames generated by a Bluff-Body burner. The central jet of methane and the annular co-axial air flow are separated by a cylindrical Bluff-Body with a large blockage ratio. The aim is to generate a recirculation zone in the wake of the Bluff-Body in order to induce a partial mixing of reactants with trapped combustion products close to the burner exit. In such configuration, the modes of stabilization of turbulent flames are often controlled by intermittent unsteady phenomena in the recirculation zone which are complex and still poorly understood. Their study requires the ability to make time-resolved measurements by the use of high-speed optical and laser diagnostics. For this purpose, high speed flame imaging (1 kHz) is performed for three operating conditions. For a constant central methane jet velocity (i.e. constant thermal power), the variation of annular air velocity allows us to cover different flames modes from a fully stabilized turbulent flame to the limit of flame blow-out. The typical structure of the turbulent flame consists in two adjacent parts: a torus flame stabilized in the recirculation zone followed by a jet-like flame developing from the end of the recirculation zone. Time-resolved flame imaging allows to reveal the occurrence of intermittent ejections of reactive pockets from the recirculation zone to the base of the main jet-like flame, ensuring its stabilization. Image processing of time-series is performed to evaluate the characteristic frequency of this periodic ejection and its variation with the annular air flow velocity. Time-series of instantaneous velocity fields in the flames are obtained by 5 kHz Particle Image Velocimetry (PIV). Their analyses show the original structure of the flow downstream the Bluff-body burner, consisting in a highly turbulent internal recirculation zone surrounded by the centripetal annular air flow and pierced by the methane central jet. Comparison between high speed flame imaging and PIV measurements allow to determine correlations between the periodic burning pockets ejection and some features of the instantaneous velocity fields in this region, in order to fully describe this physical phenomenon controlling the stabilization of the turbulent flame.

Introduction
The requirement of the increase of efficiency and the pollutants reduction in combustion systems is still an essential task today for industrial burner manufacturers and furnaces users. Recent innovative combustion regimes with low pollutants emissions and high energy efficiency usually operate with turbulent flames close to limits of stability. It is then essential to have a deeper understanding of physical phenomena leading to flame stabilization in order to be able to master, control and enhance it.
Bluff-body configuration is well adapted for the stabilization of non-premixed flames in industrial applications, such as in gas turbines, ramjets and furnaces [1, 2]. The internal recirculation zone generated by the wake effect of the flow downstream of the bluff-body induces then the partially mixing of the fuel with oxidant. Caetano et al. and Masri et al. in their studies have observed two vortices in the recirculation zone: the inner recirculation vortex (or central jet driven) is located on the side of the fuel jet whereas the outer recirculation vortex (or air driven) is located at the edge of the recirculation zone, radially further away from the axis, in contact with the annular flow [3, 4]. Trapping of high-temperature combustion products in the recirculation zone brings the necessary heat for the stabilization of the flame [5-7].

The understanding of these stabilization phenomena in turbulent flames requires the ability to perform time-resolved measurements by use of high-rate (HR) optical and laser diagnostics. Morales et al. have investigated experimentally lean flame blowout within a high-speed combustor to analyze the temporal extinction dynamics of turbulent premixed bluff-body flames [8]. The lean blowout process is captured temporally using simultaneous high-speed PIV and CH*chemiluminescence. The evolution of the flame structure, flow field, and the resulting flame strain rate are analyzed throughout extinction. This study shows that global extinction can be predicted with a Karlovitz number, only after Ka exceeds 2.4 does the flame structure undergo noticeable necking and the flame begins to extinguish. Similarly in his work, Mokaddem used the flame imaging technique with a high acquisition rate (2000 images/s), to visualize the displacement of burning pockets of the Bluff-Body burner flame [7]. Their results show that these structures provide the heat and reactive species necessary for the downstream jet-like flame stabilization. The flame–vortex dynamics are found to be the main driving mechanism of flame extinction. Furthermore, Tong et al. have studied flame stabilization mechanisms of a turbulent flame stabilized by combinations of swirl flow and bluff-body [2]. The flow is captured using high-speed PIV, while the flame structures were visualized by high-speed CH_2O PLIF and CH^* chemiluminescence. The global CO emissions from the flames were collected as well. They have found that the position of the outer recirculation zone is affected by the size of the bluff-body and the swirl strength. Also the recirculation zone determines the flame structures and the global CO emission levels. With a larger bluff-body, the air driven recirculation zone is located closer to the burner exit. The stabilization phenomenon is then controlled by heat transfers occurring in the recirculation zone. However, even if heat transfers play an important role, they cannot be separated from the wake aerodynamics, especially in the case of non-premixed flames, for which fluid mechanics will manage reactants residence times in the recirculation zone and thus influence the mixing process [9, 10].
In this configuration, the modes of stabilization of turbulent flames consist usually in unsteady phenomena in the internal recirculation zone which are complex and still poorly understood. Ejection of burning pockets from recirculation zone may be periodic and could be correlated with the complex aerodynamic structure of the flow induced by the bluff-body and the periodic burning pockets ejection. In the present study aerodynamics and flame structures are correlated for a turbulent non-premixed methane-air flame stabilized on a bluff-body burner, by means of coupling HR PIV with flame imaging.

1. Experimental setup

1.1. Burner configuration

To investigate turbulent flame stabilization, a bluff-body burner consisting of two coaxial jets is set up. The experimental device is presented in Figure 1. Methane is injected in the central jet (D_j = 8 mm) while air is injected in the annular one (D_a = 55 mm). The D_b = 48 mm-dia. bluff-body induces a large blocking ratio of 0.83.

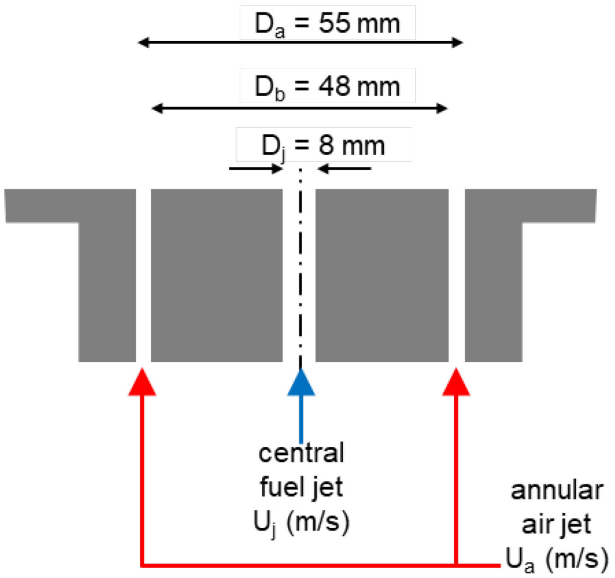

Figure 1. The Bluff-Body burner.

1.2. Stability diagram

The stability diagram is established as a first step, it provides information on the operating range of the burner as well as on the overall structures of the flames stabilized on this burner. Figure 2 shows the stability diagram of the bluff-body burner. It has been established by fixing a constant methane jet velocity and increasing the annular air velocity up to the extinction limits.

Several structures of the flames have been identified in the stability diagram and their global topologies are presented in Figure 3. Flame (a), occurring for low air velocity is dominated by the central jet of fuel. Flame (b) represents a transition flame characterized by the apparition of a small recirculation zone. Flame (c) reveals a blue cone with a base consisting of a laminar blue ring lifted from the burner exit. Both are broad and surround a laminar soot diffusion core. In flame (d) for low methane jet velocity and large annular air velocity, the fuel is mixed with the recirculating air and the whole is burnt before leaving the recirculation area. The flame structure (e) shows a flame leading edge anchored to the aerodynamic internal recirculation zone induced by the bluff-body wake. A jet-like flame is stabilized downstream of this leading edge. This flame structure, especially investigated in this work, is particularly of interest because it corresponds to typical operating conditions in practical burners and it may present intermittent phenomena. Flame (f) represents a lifted flame completely detached from the burner nozzle when the jet velocity of the flame is over a critical value, around 20 m/s in the present case. Upper limit of the stability diagram corresponds to the limit of flame blow-out (g).

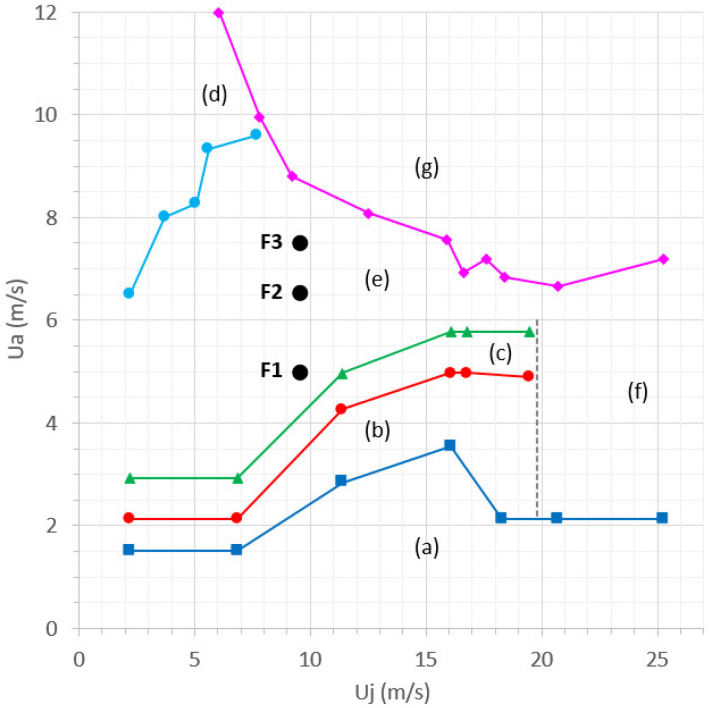

Figure 2. Stability diagram: (a) cylindrical flame, (b) Transition flame, (c) Ring laminar flame, (d) Recirculating flame, (e) long turbulent attached flame, (f) Lifted flame, (g) Extinction. F1, F2 and F3 refer to operating conditions studied in details in the present work.

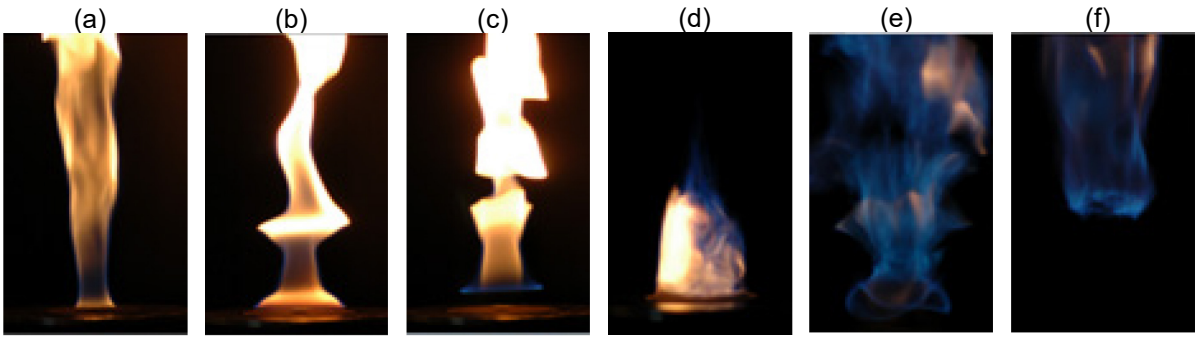

Figure 3. Direct flame visualizations of the different combustion regimes.

The operating conditions chosen for detailed characterization are established for a constant central methane jet velocity (U_j=9.6 m/s) and a variation of annular air velocity from U_a= 5.0 to 7.5 m/s (Figure 2). Three “type (e)” flames are retained from a fully stabilized turbulent flame (F1) chosen as reference case to a flame close to the blow-out limit (F3) passing by another stable flame (F2). The corresponding operating conditions are presented in Table 1. The air flow Reynolds number Re_a is determined from the diameter of the bluff-body.

Table 1. Operating conditions.

Uj (m/s)	Re_j	U_a (m/s)	Re_a	Flame
9.6	4293	5.0	16170	F1
		6.5	21024	F2
		7.5	24258	F3

1.3. Optical diagnostics

The flow and flame structures are characterized by means of the coupling of high-rate PIV and time-resolved flame emission.

The HR-PIV setup consists of a double cavity Nd:Ylf laser (Dual-DARWIN-527100-M 30 mJ @ 527 nm). A vertical laser sheet is formed by combining a spherical lens (f = 1000mm) and a cylindrical lens (f = 40mm). The laser sheet is carefully adjusted to cross the median plane of the burner and its height is around 130 mm from the burner exit. The air and methane flows are independently seeded with solid zirconium oxide particles (5 µm mean diameter) that survives the reaction zone (melting point of 2988 K). The reactants flowrates are controlled by mass flowmeters before flowing into the two fluidized beds seeding machines, allowing a careful and balanced adjustment of the particle density in each flow. Particle images are collected with a Phantom V25 CMOS camera (1280 x 800 pixels) equipped with a Nikkor 50mm (f/1.2) and an interferential filter (centered on 527 nm). The measurement analysis area corresponds to a surface of 120 mm × 150 mm and the spatial resolution is 93 µm/pix. The acquisition rate is fixed to 5 kHz. Velocity fields are obtained by a laboratory property PIV cross-correlation algorithm [11, 12]. A multi-pass subpixel shift correlation algorithm has been used. Initial pass is computed with an interrogation window size of 16 × 32 pixels the final pass is fixed to 8 × 32 pixels (0.74 × 2.96mm²) with an overlap of 50% × 25%. Intermediate filtering is based on a minimum value of Signal to Noise Ratio (SNR) and a median filter that rejects most of non-valid vectors and resulting in instantaneous fields with more than 95% validated vectors.

The flame emission is collected through a Phantom V9 high-speed camera equipped with a double stage HiCATT 25 intensifier and a UV Cerco 105 mm lens (f/2.8). An acquisition rate at 1 kHz with a gate of 140 µs are chosen as the best compromise between signal level and time integration. The spatial resolution is 113.6 µm/pix.

The high speed camera and intensifier are synchronized with the PIV laser and camera by means of a BNC-555 delay generator. Simultaneous time series of 1.5 seconds duration are recorded.

2. Aerodynamic characterization

The mean velocity field obtained for F1 flame is presented in Figure 4. The average of 7500 instantaneous velocity fields ensures the convergence of the statistics.

Three regions can be distinguished in the flow. A first zone corresponds to the recirculation zone from the nozzle of the burner up to z = 40mm. In a second zone, between 40 mm and 60 mm, the air flow streamlines converge towards the centerline. The last zone located from 60 mm and downstream corresponds to the development of the whole flow as a jet.

The recirculation zone is of particular importance in such a configuration. It is established between the central methane jet and the annular air jet and is defined by two toroidal vortices. The first large centripetal vortex is piloted by air jet and the second, smaller and centrifugal is piloted by the methane jet. These two vortices can be found in various non-premixed bluff-body configurations whatever the blocking ratio, the momentum ratio, in confined or free flow [5, 8]. The stagnation point gives the downstream boundary of the recirculation zone (respectively at r = -8 mm z = 40 mm and r = 9 mm z = 41 mm on left and right sides), which is close to the bluff-body diameter.

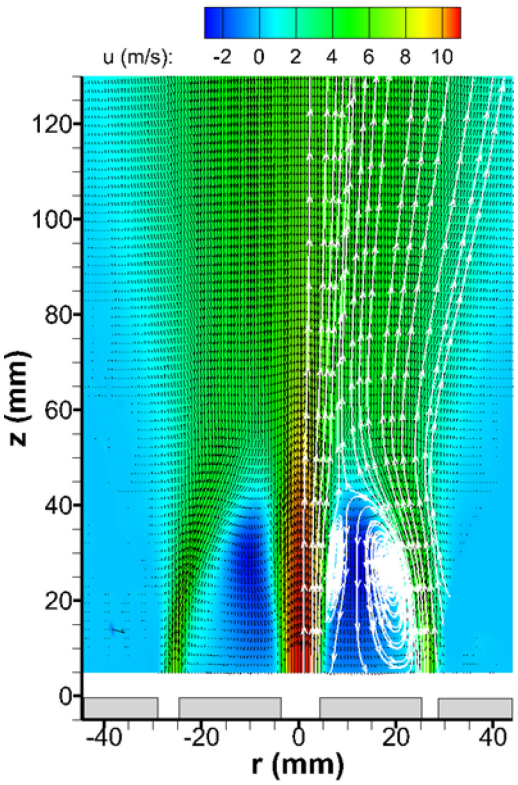

Figure 4. Time averaged axial velocity field and mean streamlines, F1 flame.

3. Mean structure of the flame

The global morphology of the flame is obtained by OH* chemiluminescence imaging. The signal is collected with an ICCD Princeton PI-MAX 4 camera with a 16-bit 1024×1024 px² sensor, equipped with a UV Sodern 105 mm lens (f/2.8) and a UG11 filter covering a 180×180 mm² domain (175 µm/px). A mean image obtained from 1000 single shot images (60 µs) is presented in Figure 5 for flame F1. From the burner exit, the mean reaction zone is located at the external border of the recirculation zone. Downstream in the flow, a mean jet-like flame is developed in continuity. Similar topology of the mean flame is observed for the other operating conditions (F2 and F3) with higher lift-off location of the flame in the recirculation zone.

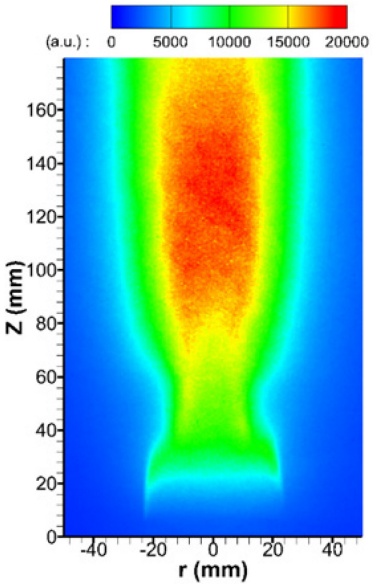

Figure 5. Averaged OH* chemiluminescence image from 1000 images, F1 flame.

Short-gated high-rate flame imaging is then used to get the turbulent flame structures and follow their evolution with time. Figure 6 shows a series of eighteen flames images, each separated with 2 ms. In

the recirculation zone, the leading edge of the flame is seen to be lifted and anchored at the inner side of the annular air jet, as also noticed on the picture presented in Figure 3. Downstream, large regions of flame extinction are observed between the recirculation zone and the main trailing flame. On the eighteen successive flame images, a reactive pocket is detached from the flame leading edge, ejected from the recirculation zone and then transported by the flow, till the downstream zone of the depleted jet flame which is re-ignited by the flame pocket. This seems to be an intermittent phenomenon more or less observable on the time series depending on the operating conditions.

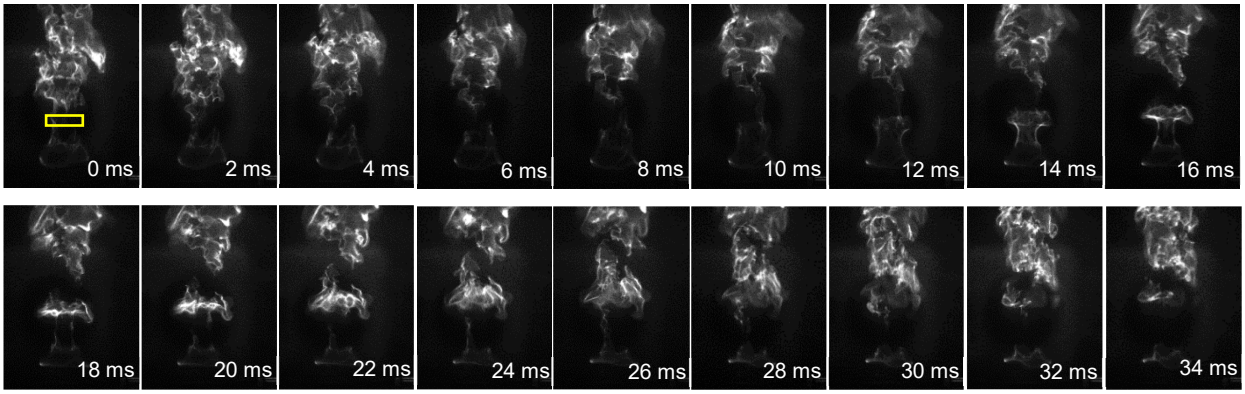

Figure 6. A short sequence of one time series of 1 kHz images of the F1 flame (1 image over 2 is shown).

4. Frequency determination of reactive pockets ejection

The presence of a characteristic frequency of the reactive kernels ejection is evaluated by post-processing of the flame emission images. Firstly, a standard deviation (std) image is obtained by subtracting the mean image on each instantaneous image of the time series. Then, the flame intensity is averaged in a specific area of 8 × 3.4 mm^2 (see Figure 6, yellow area) for each instantaneous image. This area is centered on point r=0 mm, z= 50 mm on top of the recirculation zone. A temporal evolution of F2 flame emission intensity as a function of time is shown in Figure 7. The evolution of the grey level extracted from the analysis window clearly shows the highly fluctuating nature of the turbulent flame.

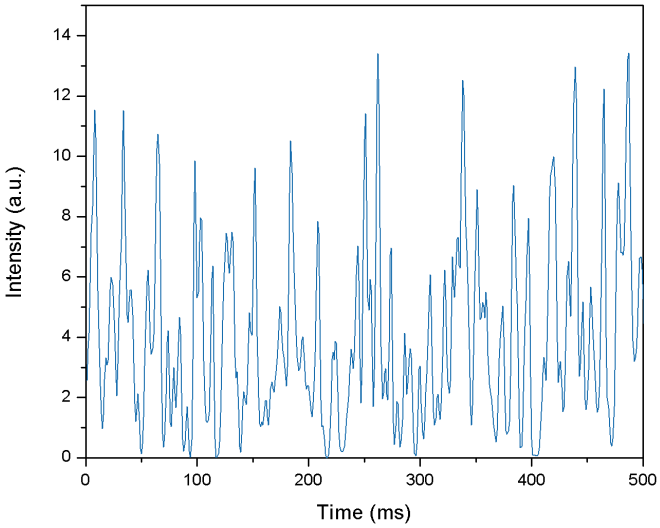

Figure 7. Temporal follow-up of the average flame intensity, F2 flame.

The characteristic frequency of a potential intermittent phenomenon is determined by means of a spectral analysis of the filtered signal. One example of FFT profile obtained for the F2 flame is presented in Figure 8. One clearly sees the presence of a peak which allows to quantify the frequency characterizing the periodic kernel ejection. This procedure is applied on three time series for each studied flame and the characteristic frequencies are gathered in Table 2.

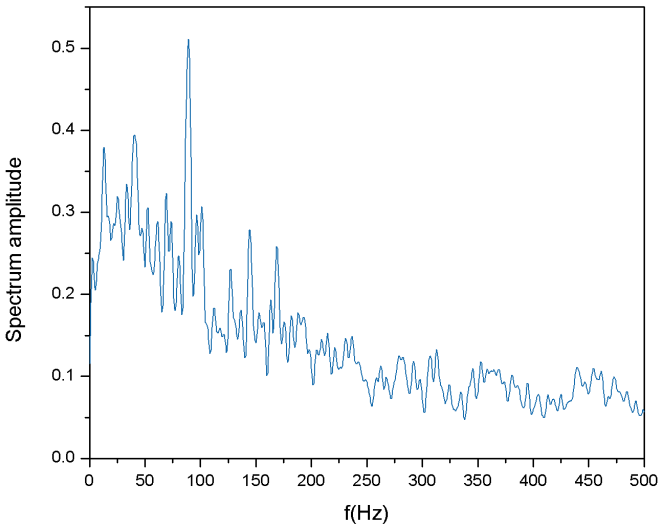

Figure 8. FFT profile obtained for the F2 flame.

Similar results are obtained for other position and size of the analysis window on the top of the recirculation zone. A typical frequency of 70 Hz is determined for F1 flame and a larger value of 90 Hz is observed for F2 flame due to the increase of air flowrate. This demonstrates the intermittent feature of the ejection of burning pockets from the recirculation zone to the main flame base. The periodic event seems to be correlated to the air flow aerodynamics since its characteristic frequency increases with air velocity. In the case of flame F3, close to the extinction limits, the flame structure does no more exhibits any periodic behavior as no characteristic frequency could be extracted from any flame emission images time-series.

5. Time resolved analysis of the aerodynamic structures

A sequence of successive instantaneous velocity fields obtained by PIV is presented Figure 9. The aerodynamics characteristic frequency is evaluated by extracting and averaging the radial component of the instantaneous velocity in a selected window positioned between the air and methane jets at z = 50 mm, r = 10 mm. The window area is 4.4 × 4.4 mm^2 for each instantaneous field. The windows size has been varied to ensure the reliability of the results. As previously done for flame imaging, the potential intermittent phenomena are determined by the spectral analysis of the time evolution. This procedure is applied on each operating condition, and the characteristic frequencies obtained for each flame type are presented in Table 2.

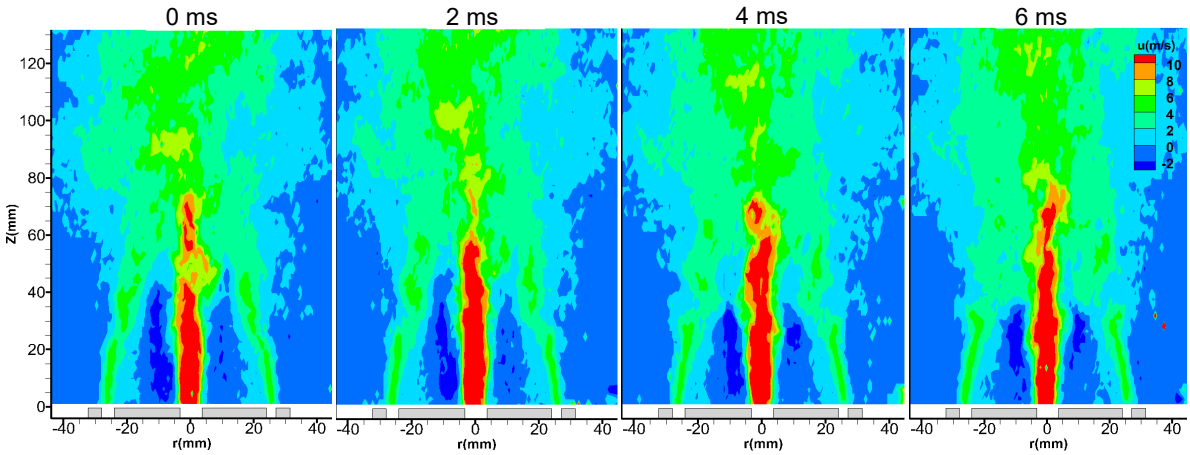

Figure 9. Sequence of instantaneous axial velocity fields obtained by 5 kHz PIV (1 over 10 successive fields is shown).

Table 2. Characteristic frequencies obtained from flame imaging and PIV.

	Frequency (Hz)	
Flame Type	Flame Imaging	PIV
F1	70 ± 3	67 ± 2
F2	90 ± 3	91 ± 2
F3	---	130 ± 2

The results show a perfect matching between the frequencies determined by PIV and by flame imaging for both stable F1 and F2 flames. This result points out the strong correlation of the aerodynamics with the periodic flame pocket ejection. As the air velocity increases (F1 to F3), the aerodynamics frequency increases. For the F3 flame, a high frequency is determined on each PIV time series whereas no frequency is obtained on flames images. The flame local detachment, in conditions close to blow-out, does not show any periodicity and the ejection of reactive zone cannot be correlated to aerodynamics structures, for these conditions. Nevertheless, the frequencies obtained from PIV measurements represent the intermittent aerodynamics features of the recirculation zone generated by the annular turbulent flow. The Strouhal number, characterizing the intermittent event of this flow is expressed as:

$St_h = \frac{f \cdot D_b}{U_a}$ based on the air velocity U_a and bluff-body diameter D_b.

Flames F1 and F2 presents similar St_h number about 0.67. This value can be linked to the natural instability of the annular air jet and corresponds to the jet preferred mode, resulting in the formation of regular vortical rings. Several studies have also shown that St_h number corresponding to the preferred mode of the jet lies in the range 0.3 - 0.8 [13-16]. These vortices, generated at the external base of the annular flow, feed the air driven recirculation zone and interact with the flame tube anchored downstream of the flame leading edge. The strong strain imposed by the vortex interaction on the flame leads to local extinction and periodic pockets ejection. In the case of F3 conditions, flame imaging does not present any characteristic frequency. The ratio $\frac{f}{U_a}$ and thus the St_h number, exceeds the value obtained for both F1 and F2 cases. The F3 flame does not seem to be controlled by aerodynamics. Under these conditions, the extinction limit is reached.

Conclusion

Turbulent Bluff-body flames stabilization phenomena were studied in the present study. The configuration studied is a non-premixed coaxial flow of air and methane. The results show that stabilization of combustion is controlled by the presence of the recirculation zone which induces some periodic ejection of burning pockets allowing ignition of the main trailing flame downstream in the flow. The phenomenon of ejection of flame pockets has a characteristic frequency, which depends on the annular air velocity injection. No specific frequency can be determined for flame close to the extinction limit.

The original flow structure downstream of the Bluff-Body burner is characterized by high-rate PIV. It consists primarily of an internal recirculation area which is defined by two vortices. The first one - a large centripetal vortex - is piloted by the annular air flow and the second one - smaller and centrifugal - is piloted by the central methane jet. Instantaneous velocity periodicity has led to the burning pockets frequency determinations which perfectly match with frequency values obtained from high-rate flame imaging for stable flames. This correlation is no more observed for a flame regime close to limit of extinction.

Acknowledgments

The study is performed in the framework of the ‘PASTEC' project with the financial support of ANR (ANR-16- CE22-0005- 02).

References

[1] Beér JM, Chigier NA, *Combustion Aerodynamics*, Applied Science Publishers Ltd, (1972).

[2] Tong, Y., Liu, X., Wang, Z., Richter, M., & Klingmann, J, Experimental and numerical study on bluff-body and swirl stabilized diffusion flames, *Fuel* 217 (2018) 352–364.

[3] Caetano, N. R., & Silva, L. F., A comparative experimental study of turbulent non premixed flames stabilized by a bluff-body burner, *Experimental Thermal and Fluid Science* 63, (2015) 20-33.
[4] A.R. Masri, R.W. Bilger, Turbulent diffusion flames of hydrocarbon fuels stabilized on a bluff body, *Symp. (Int.) Combust.* 20 (1985) 319.
[5] Susset, K. Mokaddem, D.W. Kendrick, J.C. Rolon, D. Jaffré, D. Honoré, M. Perrin, C. Gray, J.B. Richon, Convenient laser diagnostics for aerodynamic and chemical study of axisymetric non-premixed Bluff-Body burner flames. *In: Developments in Laser Techniques and Fluid Mechanics. Selected Papers from the 8th International Symposium Lisbon*, 1997.
[6] Susset, M. Trinité, D. Honoré, D. Jaffré, M. Perrin. Experimental investigation of spatio-temporal correlation between aerodynamic and flame front location in an axisymetric non premixed bluff body burner flame. *Ninth Int. Symposium on Applications of Laser Techniques to Fluid Mechanics*. July 13th-16th, Lisbon, Portugal, 1998.
[7] Mokaddem K., Contribution à la validation expérimentale de deux modèles de combustion turbulente, Ecole Centrale de Paris, 1997 Ph.D. Thesis.
[8] Morales, A. J., Lasky, I. M., Geikie, M. K., Engelmann, C. A., & Ahmed, K. A., Mechanisms of flame extinction and lean blowout of bluff body stabilized flames, *Combustion and Flame*, (2019) 203, 31–45.
[9] Nguyen, H. T., Etude expérimentale de l'influence de la geometrie du stabilisateur sur le développement d'une flamme non premlangée, Ecole Centrale de Lyon, (1999) Ph.D. Thesis
[10] Esquiva-Dano I., H.T. Nguyen, D. Escudie, Influence of a bluff-body's shape on the stabilization regime of non-premixed flames, *Combust. Flame* 127 (2001) 2167.
[11] Lecordier, B. & Trinite, M., Advanced PIV algorithms with image distortion validation and comparison using synthetic images of turbulent flow *in 'Particle Image Velocimetry: Recent Improvements'*, Springer, (2004) pp. 115-132.
[12] Lecordier, B.; Demare, D.; Vervisch, L. M. J.; Reveillon, J. & Trinite, M., 'Estimation of the accuracy of PIV treatments for turbulent flow studies by direct numerical simulation of multi-phase flow', *Measurement Science and Technology* 12(9), (2001) 1382--1391.
[13] Danlos A., Lalizel G., Patte-Rouland B. Experimental characterization of the initial zone of an annular jet with a very large diameter ratio. *Experiments in Fluids*, 2013.
[14] Crow SC, Champagne FH. Orderly structure in jet turbulence.*J Fluid Mech* 48, (1971) 547–591
[15] Birbaud AL, Durox D, Ducruix S, Candel S. Dynamics of free jets submitted to upstream acoustic modulations. *Phys Fluids* 19 (2007) (1).
[16] Gutmark E, Ho CM. On the preferred modes and the spreading rate of jets. *Phys Fluids* 26, (1983) 2932–2938